Chemistry–A European Journal

Research Article
doi.org/10.1002/chem.202301853

Chemistry Europe
European Chemical Societies Publishing

www.chemeurj.org

Special Collection

Elucidating the Excited State Behavior of Pyridyl Pyridinium Systems via Computational and Transient Absorption Studies of Tetrahedral Multichromophoric Arrays and their Model Compounds

Barbara Ventura,[a] Daniele Veclani,[a] Alessandro Venturini,[a] Nicola Armaroli,*[a] Massimo Baroncini,[b] Paola Ceroni,[c] and Marianna Marchini*[c]

Dedicated to Prof. Maurizio Prato on the occasion of his 70th birthday.

The tetrahedral shape-persistent molecule $\mathbf{1}^{4+}$, containing four identical pyridyl pyridinium units connected via a sp^3 hybridized carbon atom, has been investigated in detail by means of steady-state and time resolved spectroscopy. Remarkable photophysical properties are observed, particularly in comparison with protonated and methylated analogues ($\mathbf{1H_4}^{8+}$, $\mathbf{1Me_4}^{8+}$), which exhibit substantially shorter excited state lifetimes and lower emission quantum yields. Theoretical studies have rationalized the behavior of the tetrameric molecules relative to the monomers, with DFT and TD-DFT calculations corroborating steady-state (absorption and emission) and transient absorption spectra. The behavior of the monomeric compounds (each consisting in one of the four identical subunits of the tetramers, i.e., $\mathbf{2}^{+}$, $\mathbf{2H}^{2+}$ and $\mathbf{2Me}^{2+}$) considerably differs from that of the tetramers, indicating a strong electronic interaction between the subunits in the tetrameric species, likely promoted by the homoconjugation through the connecting sp^3 C atom. $\mathbf{2}^{+}$ is characterized by a peculiar S_1-S_2 excited state inversion, whereas the short-lived emitting S_1 state of $\mathbf{2H}^{2+}$ and $\mathbf{2Me}^{2+}$ exhibits a partial charge-transfer character, as substantiated by spectro-electrochemical studies. Among the six investigated systems, only $\mathbf{1}^{4+}$ is a sizeable luminophore ($\Phi_{em} = 0.15$), which is related to the peculiar features of its singlet state.

Introduction

Shape-persistent multichromophoric systems may exhibit the emergence of new properties arising from the interaction between the constituent subunits.[1,2,3,4] Notably, this arrangement allows a precise control of the interchromophoric distance and the relative orientation of the chromophores. In order to clarify how the spatial arrangement affects the properties of the whole system, it is essential to compare the chemical and photophysical properties of the individual chromophoric units with those of the multichromophoric arrays.[5,6,7]

Pyridinium and bipyridinium chromophores (the latter also known as viologens, namely, 1,1′-disubstituted-4,4-bipyridinium salts) are extensively studied for their remarkable photochemical and electrochemical properties.[8] They have been explored as components for molecular batteries, electrochromic displays, redox mediators and redox sensors.[9,10,11] They are also widely employed as electron-acceptor recognition sites and redox switching units in supramolecular systems[12] and as coordinating sites for transition metals such as ruthenium.[13] More recently, they found application in the field of photoredox catalysis.[14] Furthermore, there is great interest in designing new types of pyridiniums and bipyridiniums that behave not only as good electrophores and chromophores, but also offer the chance to expand the molecular scaffold of their π-system.[15]

In this study, three different large tetrameric molecules based on pyridinium and bipyridinium components have been

[a] Dr. B. Ventura, Dr. D. Veclani, Dr. A. Venturini, Dr. N. Armaroli
Istituto per la Sintesi Organica e la Fotoreattività
Consiglio Nazionale delle Ricerche (ISOF-CNR)
Via P. Gobetti 101, 40129 Bologna (Italy)
E-mail: nicola.armaroli@isof.cnr.it
Homepage: http://www.isof.cnr.it/armaroli_nicola/

[b] Prof. M. Baroncini
CLAN-Center for Light Activated Nanostructures
Consiglio Nazionale delle Ricerche (ISOF-CNR)
Via P. Gobetti 101, 40129 Bologna (Italy)
and
Dipartimento di Scienze e Tecnologie Agro-alimentari
Università di Bologna
Viale G. Fanin 50, 40127 Bologna (Italy)

[c] Prof. P. Ceroni, Dr. M. Marchini
Dipartimento di Chimica "G. Ciamician"
Università di Bologna
Via F. Selmi 2, 40126, Bologna (Italy)
E-mail: marianna.marchini@unibo.it
Homepage: http://www.unibo.it/sitoweb/marianna.marchini2

Supporting information for this article is available on the WWW under https://doi.org/10.1002/chem.202301853

This article is part of a joint Special Collection in honor of Maurizio Prato.

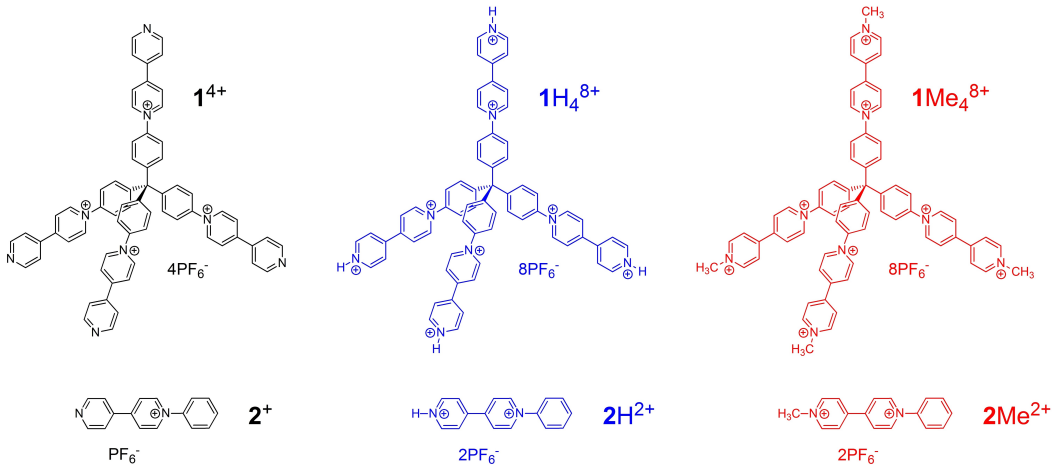

Scheme 1. Structure of the studied tetrameric species and of the related monomeric compounds.

explored: $\mathbf{1}^{4+}$, made of pyridyl pyridinium units, which have been so far barely investigated in the literature from the photophysical point of view; $\mathbf{1H_4}^{8+}$ and $\mathbf{1Me_4}^{8+}$, tetramers based on the more classical bipyridinium chromophores in their protonated and methylated forms, respectively. Despite the marked structural similarity of the three systems, their excited state dynamics is largely affected by the type of subunit (i.e., pyridyl pyridinium vs. bipyridinium) and their properties are uniquely affected by the tetrameric arrangement of the four arms. Notably, such properties are significantly different from those of the related monomeric units.

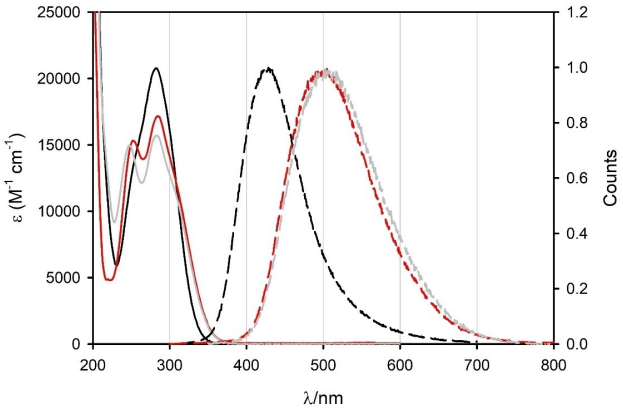

Figure 1. Absorption (solid lines) and normalized emission spectra (dashed lines) of $\mathbf{2}^{+}$ (black lines), $\mathbf{2H}^{2+}$ (grey lines) and $\mathbf{2Me}^{2+}$ (red lines) in acetonitrile at 298 K; $\lambda_{exc} = 282$ nm.

Results and Discussion

Synthesis

The molecular structures of $\mathbf{1}^{4+}$, $\mathbf{1H_4}^{8+}$, and $\mathbf{1Me_4}^{8+}$, along with those of the related model compounds, $\mathbf{2}^{+}$, $\mathbf{2H}^{2+}$, $\mathbf{2Me}^{2+}$ are depicted in Scheme 1. The synthesis of $\mathbf{1Me_4}^{8+}$ and $\mathbf{1}^{4+}$, as well as the corresponding monomeric species, was performed according to previously published procedures.[8,16]

The fully protonated form $\mathbf{1H_4}^{8+}$ and $\mathbf{2H}^{2+}$ were obtained upon titration of $\mathbf{1}^{4+}$ and $\mathbf{2}^{+}$, via the addition of increasing amounts of triflic acid (CF_3SO_3H). In the absorption and emission spectra, a plateau appears after the addition of ca. 1 equivalent of acid in the case of monomer $\mathbf{2}^{+}$ and four equivalents of acid in the case of tetramer $\mathbf{1}^{4+}$ (Figures S1–S3).

Photophysical properties

The photophysical properties of the tetrameric and monomeric species (as hexafluorophosphate salts) were investigated in acetonitrile solution. The absorption spectrum of monomer $\mathbf{2}^{+}$ (Figure 1, black solid line) shows a band in the UV with maximum at 282 nm. The absorption spectra of $\mathbf{2H}^{+}$ and $\mathbf{2Me}^{2+}$ are very similar to each other, displaying a red-shifted onset of absorption compared to $\mathbf{2}^{+}$ and two distinct absorption maxima (Figure 1, grey and red solid lines). Concomitantly, the emission maxima of the protonated and methylated monomers are very similar and significantly red-shifted compared to that of $\mathbf{2}^{+}$ (around 30 nm, Figure 1, dashed lines). All the three monomers are weakly emissive, with a lifetime around or below 0.5 ns (Table 1).

The absorption spectrum of tetramer $\mathbf{1}^{4+}$ shows a band in the UV with maximum at 300 nm ($\varepsilon = 81500\ M^{-1}cm^{-1}$), Figure 2, which differs from that of the model compound $\mathbf{2}^{+}$, indicating that the absorption spectrum of this tetramer is not the mere superimposition of the absorption spectra of tetraphenylmethane and 4-pyridylpyridinium units, even if the epsilon is four times that of the model compound $\mathbf{2}^{+}$. A structured absorption spectrum, with the lowest absorption band centered at 317 nm, is observed when the four subunits are protonated or methylated (Figure 2, grey and red solid lines). Interestingly, $\mathbf{1}^{4+}$ displays a blue emission with a quantum yield of 15%, completely different from that of the model compound $\mathbf{2}^{+}$ and nearly 40 times more intense. On the other hand, the fluorescence bands of both $\mathbf{1H_4}^{8+}$ and $\mathbf{1Me_4}^{8+}$ are red-shifted

Table 1. Photophysical data of tetramers $\mathbf{1}^{4+}$, $\mathbf{1H_4}^{8+}$, $\mathbf{1Me_4}^{8+}$ and monomers $\mathbf{2}^{+}$, $\mathbf{2H}^{2+}$, $\mathbf{2Me}^{2+}$ in acetonitrile at 298 K and in CH_2Cl_2:CH_3OH 1:1 (v/v) rigid matrix at 77 K.

	Absorption		Emission				
	298 K		298 K			77 K	
	λ [nm]	ε [10^4 $M^{-1}cm^{-1}$]	λ [nm]	Φ_{em} [%]	τ [ns]	λ [nm]	τ [ns]
$\mathbf{2}^{+}$	282	2.07	431	0.4	<0.5	386	1.7
$\mathbf{2H}^{2+}$	282	1.56	503	1.6	<0.5	404	2.7
$\mathbf{2Me}^{2+}$	285	1.72	500	1.5	0.5	408	2.2
$\mathbf{1}^{4+}$	300	8.15	464	15[17]	1.0	403	2.3
$\mathbf{1H_4}^{8+}$	317	4.80	550	0.7	<0.5	447	3.4
$\mathbf{1Me_4}^{8+}$	317	5.21	550	1.2	<0.5	480	3.4

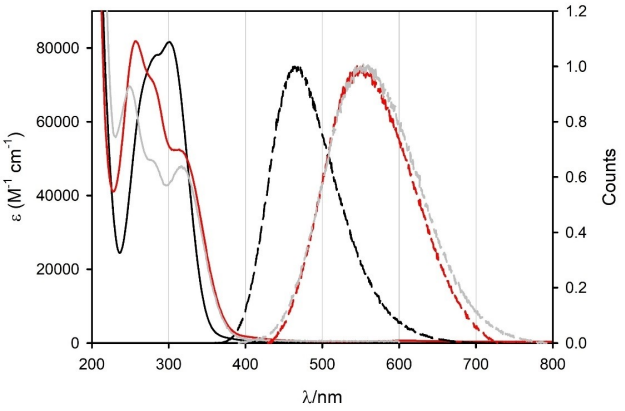

Figure 2. Absorption (solid lines) and normalized emission spectra (dashed lines) of $\mathbf{1}^{4+}$ (black lines), $\mathbf{1H_4}^{8+}$ (grey lines) and $\mathbf{1Me_4}^{8+}$ (red lines) in acetonitrile at 298 K; $\lambda_{exc}=300$ nm.

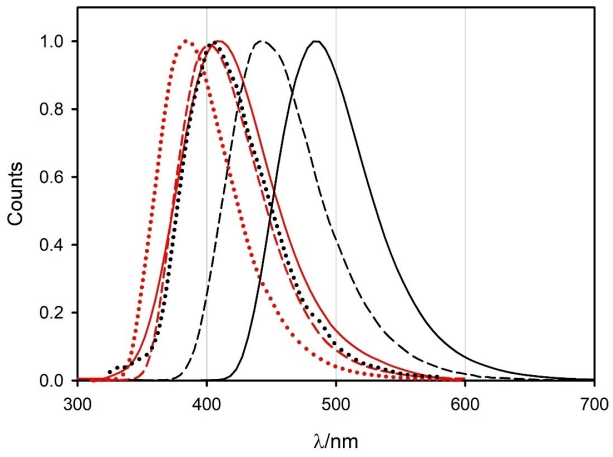

Figure 3. Normalized emission spectra in CH_2Cl_2:CH_3OH 1:1 (v/v) at 77 K of $\mathbf{2}^{+}$ (red dotted line), $\mathbf{2H}^{2+}$ (red dashed line), $\mathbf{2Me}^{2+}$ (red solid line), $\mathbf{1}^{4+}$ (black dotted line), $\mathbf{1H_4}^{8+}$ (black dashed line) and $\mathbf{1Me_4}^{8+}$ (black solid line). $\lambda_{exc}=282$ nm for monomeric species, $\lambda_{exc}=300$ nm for tetrameric ones.

by 85 nm with respect to that of $\mathbf{1}^{4+}$ (Figure 2, dashed lines) and these tetramers are very weakly emissive, similar to all the reference compounds (Table 1).

In rigid matrix at 77 K, the maxima of the emission spectra of the monomer derivatives are much closer, even though a red-shift is still observed from $\mathbf{2}^{+}$ to $\mathbf{2Me}^{2+}$ (Figure 3, red lines) with a less pronounced effect with respect to the tetrameric species. The emission trend of the tetramers at 77 K is peculiar: from the pristine $\mathbf{1}^{4+}$ to the protonated and methylated forms, a 44 and 77 nm red-shift is observed, respectively (Figure 3, black lines). Therefore, while at room temperature the fluorescence bands of $\mathbf{1H_4}^{8+}$ and $\mathbf{1Me_4}^{8+}$ peak at similar wavelengths, at 77 K the fluorescence band of $\mathbf{1Me_4}^{8+}$ is significantly red-shifted in comparison to $\mathbf{1H_4}^{8+}$. This evident difference in rigid matrix is hard to rationalize and might indicate a stronger charge transfer character of the electronic transition of $\mathbf{1H_4}^{8+}$ which, accordingly, would be blue-shifted at 77 K. It has also to be emphasized that $\mathbf{1H_4}^{8+}$ is obtained upon titration of $\mathbf{1}^{4+}$ acetonitrile solution with triflic acid, consequently the two solid matrices are not strictly identical. In addition, time-gated experiments were performed at room temperature and 77 K: none of the studied compounds show phosphorescence emission.

Theoretical studies

DFT and TD-DFT calculations of $\mathbf{2}^{+}$, $\mathbf{2Me}^{2+}$, $\mathbf{1}^{4+}$ and $\mathbf{1Me_4}^{8+}$ systems have been performed to rationalize their spectroscopic properties.

The ground state of $\mathbf{2}^{+}$ is not planar due to the steric hindrance between the hydrogens of the three rings of the molecule. Therefore, different conformations depending on the dihedral angle between the aromatic rings can be anticipated. Such conformations, given the structure of these molecules which are made of aromatic planar rings, are essentially two (Figure S4). Calculations show that the energy difference between the two conformers is 0.1 and 0.01 kcal mol^{-1} for $\mathbf{2}^{+}$ and $\mathbf{2Me}^{2+}$ respectively. Since there is no evidence that the photophysical properties are affected, we discuss only the conformers a) and c) in Figure S4.

In $\mathbf{2}^{+}$, the ground-state dihedral angle between the pyridine and pyridinium ion moiety (δ_1) is 144.3° and between pyridinium ion and phenyl moiety is 125.3 (δ_2) (Figure S4a). This molecule has three very close absorption bands, the lowest in energy peaking at 271.2 nm with an oscillator strength of 0.005 (a near zero probability). This (n→π*) HOMO–LUMO transition

involves the lone pair of the pyridinic nitrogen and the lowest π* orbital of the molecule (LUMO). The second transition is π→π* and placed at 264.6 nm, with an oscillator strength of 0.757 that involves the π HOMO-1 and the LUMO π* orbitals. The third transition, which has a low probability, involves the HOMO-2 π orbital, completely localized on the pyridine moiety of the molecule and the LUMO orbital (Figure 4a).

Optimizing from S_1 and S_2, two minima were found, with the π→π* minimum of S_2 being lower-lying than the corresponding n→π* minimum of S_1. Therefore, there is a switch along the deactivation pathways between the first two excited states, before they reach their corresponding minima (Figure 4b, *f* values). The S_2 minimum corresponds to a transition at 382.0 nm ($f=1.252$) above the ground state, which is significantly blue-shifted relative to the experimental emission. This blue shift is characteristic of the adopted level of theory[18] and therefore always occurs in all the calculations described in this work. The S_2 minimum is more planar, as shown by the calculated dihedral angles δ_1 and δ_2 (175.4° and −159.7°, respectively).

In order to give a qualitative idea of the transition to the triplet, we made calculations of Spin Orbital Coupling (SOC) from the S_1 minimum (π→π* excited state, formerly S_2). In these calculations, the two factors influencing the rate constant of intersystem crossing k_{isc} are the matrix element HSOC, $<S_n|$ HSOC $|T_m>$ (S_n and T_m are the two singlet and triplet states) and the energy difference between the two states. A significant matrix element shows the coupling between S_1 and T_4 states through the z component of the SOC operator. The two states are close in energy (Figure S5a and S5b) and the crossing involves a change of orbital type (π→π* to n→π*) in agreement with the El-Sayed rule about the rate of the intersystem crossing. The triplet phosphorescence is estimated at 581.9 nm, but it is not experimentally observed.

In the ground-state, **2**Me^{2+} is also not planar: the two dihedral angles have almost the same values calculated for $\mathbf{2}^+$ (Figure S4b). **2**Me^{2+} does not have the n→π* band; indeed, the three lowest bands are all π→π* in nature, with the lowest peaking at 276.6 nm and exhibiting a significant oscillator strength ($f=0.512$). The related HOMO orbital is centered on the phenyl moiety (Figure 5a).

Optimizing the system from the S_1 excited state, the corresponding π→π* minimum is obtained. In this transition, a small charge shift from the phenyl ring to the viologen unit is observed. It can be noticed that the switch with other excited states does not occur, as found for $\mathbf{2}^+$ (Figure 5b). The structure of the optimized minimum is more planar than the corresponding ground state structure ($\delta_1=173.2°$ and $\delta_2=157.2°$), as observed for $\mathbf{2}^+$. This system has a transition above the ground state of 408.7 nm with an oscillator strength of 1.177 (the experimental value is 500 nm at 298 K and 408 nm at 77 K in rigid matrix, see Table 1). The corresponding SOC calculations show that HSOC elements are very small (<1), which rules out the formation of the triplet. In any case, we have corroborated the nature of the absorption and the excited states also using single points STEOM-DLPNO-CCSD calculations of $\mathbf{2}^+$ and **2**Me^{2+} without observing any major differences (data not shown).

Due to the symmetry, the occupied orbitals with a higher energy of tetramer $\mathbf{1}^{4+}$ are degenerate into groups made of four and two orbitals. The first two groups of four orbitals represent linear combinations of the first two orbitals (HOMO and HOMO-1) of the $\mathbf{2}^+$ ground state. The geometry of an individual arm of $\mathbf{1}^{4+}$ is almost identical to that of the $\mathbf{2}^+$ molecule (Figure S6a). The first four transitions are n→π* and are degenerate with the orbitals linearly combined following the S_4 symmetry group; the transition is located at 272.6 nm (*f* from 0.000 to 0.0084). The second group of transitions corresponds to the π→π* transition of the $\mathbf{2}^+$ system. Two degenerate transitions at 271.7 nm ($f=1.105$, Figure 6) have a high probability.

The transitions are all energetically very close. The π→π*, with a *f* value greater than 1, have the highest probability. This is also proved by the fact that, once the geometry is optimized, the system is arranged in such a way that the first excited state is a π→π* transition and concerns only one arm of the tetramer, since the individual arms are too far apart to interact. The $\mathbf{2}^+$ moiety of the emitting arm changes the geometry becoming almost identical to that of $\mathbf{2}^+$ in the excited state (Figure S7a).

From the comparison between $\mathbf{2}^+$ and $\mathbf{1}^{4+}$, the molar absorption coefficient (ε) of the tetramer $\mathbf{1}^{4+}$ at the spectral

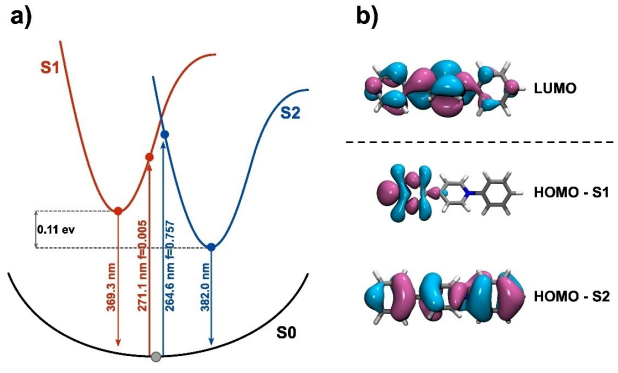

Figure 4. a) Qualitative description of the absorption and emission transitions of $\mathbf{2}^+$ along with energy and oscillator strength (*f*). Red line represents the lowest transition to S_1, blue line the transition to S_2. b) Orbitals of $\mathbf{2}^+$ involved in the two lowest transitions.

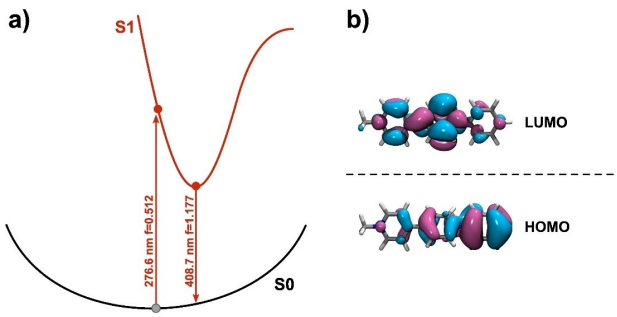

Figure 5. a) Qualitative description of the absorption and emission transitions of **2**Me^{2+} along with energy and oscillator strength (*f*). b) Orbitals of **2**Me^{2+} involved in the two lowest transitions.

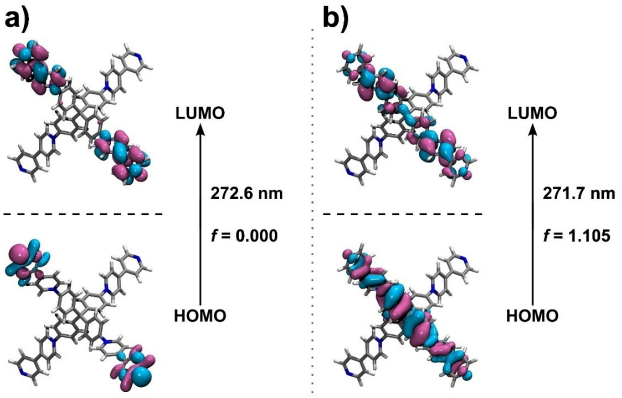

Figure 6. a) n→π* orbitals (a sample) and energies of the four lowest transitions of $\mathbf{1}^{4}$; b) a sample of π→π* orbitals involved in the transitions with the highest probability.

peak is four times that of $\mathbf{2}^{+}$, in agreement with the experiment. From the calculations, the $\mathbf{1}^{4+}$ lowest excited state is located at 387.7 nm. Similar to $\mathbf{2}^{+}$, this value is blue-shifted relative to the experimental one, which is centered at 465 nm (403 nm at 77 K in Table 1). Moreover, calculations show a red-shift of 5.7 nm between $\mathbf{1}^{4+}$ and $\mathbf{2}^{+}$ (in comparison with an experimental value of 33 nm at 298 K and 17 nm at 77 K in rigid matrix), Figure 7a.

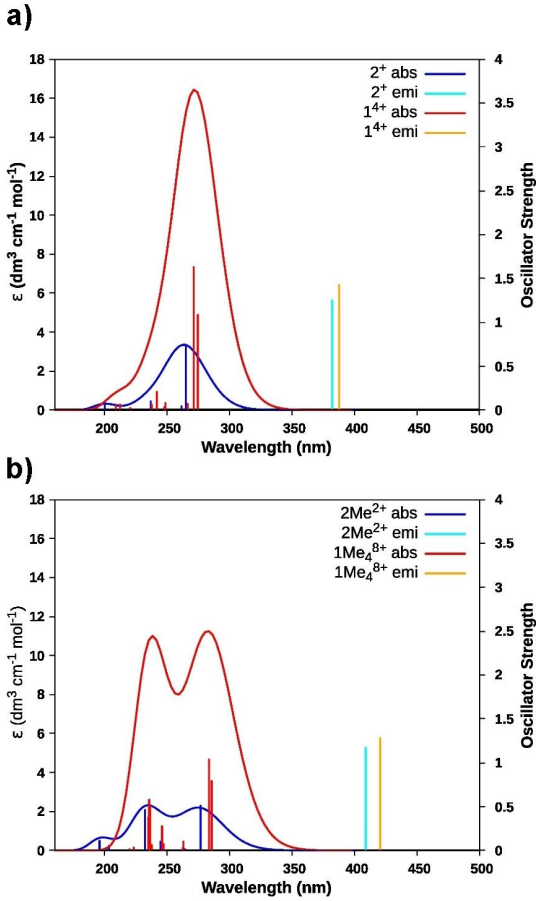

Figure 7. Comparison of the calculated absorption and emission spectra of a) $\mathbf{2}^{+}$ and $\mathbf{1}^{4+}$ and b) $\mathbf{2Me}^{2+}$ and $\mathbf{1Me}_4^{8+}$.

This shift is easily explained by the variation of the corresponding dipoles and by the conjugation of the orbitals involved in the transition with those of the central carbon, as seen in Figure 6b.

Many of the considerations made for $\mathbf{1}^{4+}$ are valid also for the tetramer $\mathbf{1Me}_4^{8+}$. In the ground state, there is a S_4 symmetry and the degenerate orbitals can be split into subgroups of two and four. On the other hand, all the valence orbitals involved in the lowest transitions are π in nature (Figure 8).

The first two transitions are π→π*, with the orbitals linearly combined following the symmetry of the molecule. The value of the first two transitions is 282.3 nm ($f = 0.777$).

Once relaxed, the geometry of the lowest excited state is found on an individual arm, which has almost the same geometry of $\mathbf{2Me}^{2+}$ and entails the same orbitals involved in the excitation (Figure S7b). Similar to the case of $\mathbf{2}^{+}$ and $\mathbf{1}^{4+}$, the calculated maximum of the excited state of $\mathbf{1Me}_4^{8+}$ is red-shifted with respect to $\mathbf{2Me}^{2+}$(11.2 nm), Figure 7b. The calculated energy of the transition is 419.9 nm with and oscillator strength of 1.280. Variation of the dipole and conjugation with the central carbon orbitals are the most likely explanation of the observed shift (Figure 8).

Transient absorption analysis

Ultrafast pump-and probe experiments on the three tetramers and the related monomers have been performed to elucidate the excited state dynamics of the systems and to rationalize

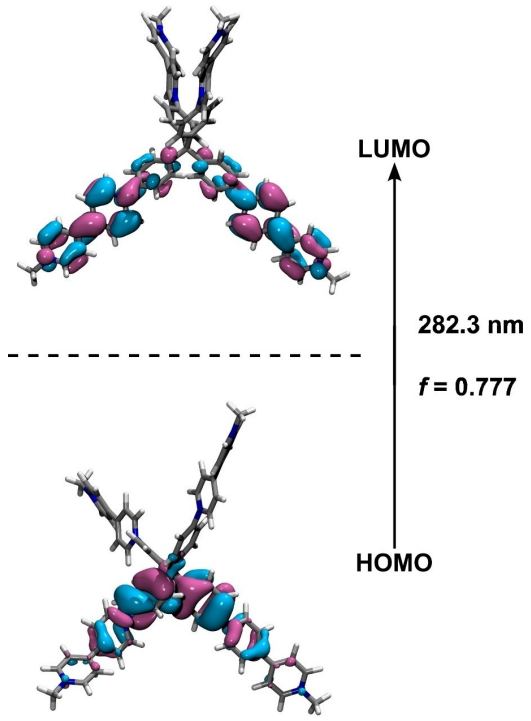

Figure 8. Electronic absorption of $\mathbf{1Me}_4^{8+}$ with a sample of the orbitals involved in the two lowest transitions.

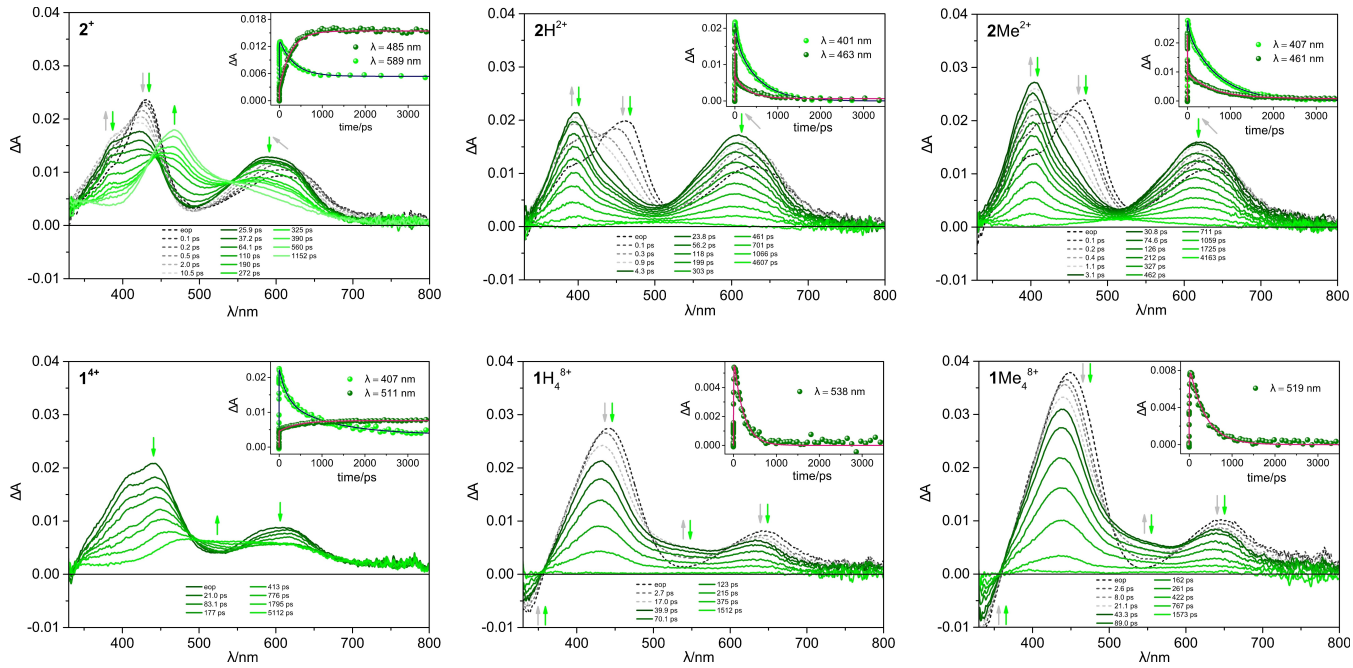

Figure 9. Transient absorption spectra of the different compounds in acetonitrile at the end-of-pulse (eop) and at different delays. Excitation at 300 nm (A_{300} = 0.20, 0.2 cm optical path, 2 μJ/pulse). Kinetic analysis at significant wavelengths is reported in the insets. The spectra associated with the first and second process, when present, are evidenced in grey (dash) and green colour scales, respectively.

their different photophysical behavior. Measurements have been performed in acetonitrile, upon excitation at 300 nm.

Figure 9 collects and compares the transient absorption behavior of all the examined compounds. Monomer $\mathbf{2}^{+}$ shows an end-of-pulse spectrum characterized by two positive bands with maxima at 431 and 604 nm. The evolution of the signal is biphasic: a first rapid process leads to the disappearance of the band at 431 nm with the appearance of a blue-shifted shoulder at 385 nm; at the same time a rise and blue-shift of the band at 604 nm occurs. The process has a time constant of 5 ps (Table 2).[18] In the second phase the signal evolves in 290 ps (Table 2, in agreement with a fluorescence lifetime $<$0.5 ns measured with the single photon counting apparatus, Table 1), towards a spectrum with a single band at ca. 470 nm that remains stable on longer timescales. In this second event, clear isosbestic points are observed. The two processes can be attributed, in accordance with theoretical results, to a $S_2 \rightarrow S_1$ singlet switch followed by population of the triplet state, whose signal is identified with the spectrum at 1152 ps, peaking at 470 nm (Figure 9 top left).

Table 2. Excited state lifetimes as determined by transient absorption spectroscopy in acetonitrile at 298 K.

	τ_1 [ps]	τ_2 [ps]
$\mathbf{2}^{+}$	5 ± 2	290 ± 30
$\mathbf{2}H^{2+}$	1.5 ± 0.5	330 ± 40
$\mathbf{2}Me^{2+}$	1.6 ± 0.4	550 ± 40
$\mathbf{1}^{4+}$	1250 ± 215	/
$\mathbf{1}H_4^{8+}$	7.2 ± 0.5	210 ± 20
$\mathbf{1}Me_4^{8+}$	10 ± 2	370 ± 20

The behavior of the monomers $\mathbf{2}H^{2+}$ and $\mathbf{2}Me^{2+}$ is quite different (Figure 9): the end-of pulse spectrum has maxima, in both cases, at ca. 465 and 630 nm, i.e., red-shifted with respect to that of $\mathbf{2}^{+}$. A biphasic behaviour is again present: in a first fast process (1.5 ps) the band at 465 nm disappears with the clear appearance of a band at ca. 400 nm, whilst the band at 630 nm rises and blue-shifts to 607 and 620 nm for $\mathbf{2}H^{2+}$ and $\mathbf{2}Me^{2+}$, respectively. The formed signal then decays to zero in 330 ps and 550 ps for the protonated and methylated derivatives, respectively (Table 2). The absence of the formation of the triplet, that mainly differentiate the excited state deactivation of the derivatives compared to parent $\mathbf{2}^{+}$, is predicted by the theoretical analysis. The lifetime of hundreds of ps agrees with the measured fluorescence lifetime of both compounds ($<$ 0.5 ns, Table 1), indicating that the species that forms within 1.5 ps is the lowest emissive singlet, which is $\pi \rightarrow \pi^*$ in nature as described by calculations for $\mathbf{2}Me^{2+}$. The transient absorption spectral features of this state, with maxima at ca. 400 and 600 nm, are similar to those obtained with spectroelectrochemical measurements (see Supporting Information for more details) and resemble the characteristics features of reduced methyl viologen species,[20,21] indicating a partial charge transfer from the phenyl to the viologen group, as confirmed by the theoretical study. The observed fast generation of this state (1.5 ps) can be attributed to internal conversion from very close higher excited states, a hypothesis corroborated by computational findings for $\mathbf{2}Me^{2+}$.

Tetramer $\mathbf{1}^{4+}$ shows the most peculiar features among all the examined compounds: a single process is observed, with

spectral changes that leads to the decrease of two bands at 440 and 615 nm and to an increase of absorption in the region 500–580 nm (isosbestic at 490 nm, Figure 9). This broad spectrum remains constant on long timescales and can be assigned to the lowest triplet excited state.[13] The decay occurs in 1.25 ns (Table 2), well matching the measured fluorescence lifetime (Table 1), and the process can be ascribed to S_1-T_1. It can be noticed that, unlike monomer $\mathbf{2}^{+}$, a fast process prior to intersystem crossing is not detected in $\mathbf{1}^{4+}$.

Tetramers $\mathbf{1}H_4^{8+}$ and $\mathbf{1}Me_4^{8+}$ show different transient spectral features compared to $\mathbf{1}^{4+}$, with end-of-pulse spectra exhibiting maxima at ca. 445 and 645 nm, which evolve rapidly with decrease of the two bands and increase of absorption in the region 500–600 nm (isosbestic points can be identified at 493 and 501 nm, respectively). This spectral transformation resembles that of parent $\mathbf{1}^{4+}$ but it occurs on completely different times scales: 7 ps for $\mathbf{1}H_4^{8+}$ and 10 ps for $\mathbf{1}Me_4^{8+}$ (Table 2). The formed signal then decays to zero in 210 ps and 370 ps (Table 2), respectively, in agreement with fluorescence lifetimes (<0.5 ns). Ground-state bleaching above 350 nm is also observable for the two derivatives thanks to a red-shifted transient absorption. The observed behaviour can be interpreted in terms of formation and decay of the emissive lowest singlet excited state.

With the only exception of $\mathbf{1}^{4+}$, where the lifetime of the lowest singlet excited state is of the order of 1 ns, transient data show that the excited state deactivation to the ground state (or triplet state) of monomers and tetramers is very fast (hundreds of ps), leading to a weaker emission. Notably, longer-lived singlet excited state and high luminescence quantum yield are observed only for $\mathbf{1}^{4+}$. This is the only system - out of the six investigated - that exhibits a regular singlet-to-triplet intersystem crossing with no singlet inversion (as the Ref. $\mathbf{2}^{+}$) or ultrafast singlet deactivation with no triplet occurrence (as the other tetramers $\mathbf{2}Me^{2+}$ and $\mathbf{1}Me_4^{8+}$). This further strengthens the correlation between theoretical and experimental data.

It is interesting to note that by inspecting in parallel the transient absorption and fluorescence spectra (i.e., spectral positions and/or shapes) of each of the three tetramers vs the related monomeric species, they are invariably different. A plausible explanation comes from electronic homoconjugation, which consists in the orbital overlap of two π-systems separated by a non-conjugated group.[16,22,23] In the tetramers, indeed, conjugation among the aromatic units located on the different arms can occur through the orbitals of the central carbon atom of the tetraphenylmethane scaffold, as observed in other tetrameric systems containing the same structural core.[24,25] This phenomenon is also supported by the theoretical results discussed above and can account for the different features observed for the tetrameric species.

Conclusions

We have characterized the photophysical properties of a shape-persistent multichromophoric molecule based on pyridyl pyridinium moieties ($\mathbf{1}^{4+}$), along with its protonated and methylated analogues. The set of tetrameric molecules bear four identical subunits, which were also investigated as single monomers in order to get a deeper insight on the behavior of the tetramers. Steady-state absorption and emission spectra, and transient absorption features are markedly different when comparing the tetramers with the model compounds, indicating an electronic interaction between the subunits in the tetrahedral arrays. The peculiar homoconjugation of the central tetraphenylmethane scaffold can be invoked to explain such a behavior.[23]

DFT and TD-DFT calculations were performed on the pyridyl pyridinium based tetramer, the methylated equivalent and the corresponding monomers. The results indicate that in monomer $\mathbf{2}^{+}$ a switch between the two lowest singlet excited states occurs with formation of an emissive π→π* singlet state, and subsequent population of a triplet state. In $\mathbf{1}^{4+}$, a π→π* transition which concerns only one arm of the tetramer is responsible for the observed emission. In the methylated monomer $\mathbf{2}Me^{2+}$ a π→π* transition with a small charge shift is predicted, while for the corresponding tetramer $\mathbf{1}Me_4^{8+}$ the lowest excited state has almost the same geometry of the individual arm $\mathbf{2}Me^{2+}$, with the same orbitals involved in excitation and emission. Notably, the theoretical results well predict the emission shifts observed experimentally and agree with the excited state characterization resulting from transient absorption analysis.

Overall, the present study clarifies the pattern of light-induced processes of pyridinium and bipyridinium (i.e., viologen) systems on the ultrafast scale, highlighting the peculiar excited state dynamics of related shape-persistent multichromophoric arrays. This opens the route for the construction of spatially controlled architectures based on these moieties, which may exhibit tailored luminescence and excited-state properties.

Experimental Section

Materials and methods: Compounds $\mathbf{1}^{4+}$, $\mathbf{1}Me_4^{8+}$, $\mathbf{2}^{+}$, and $\mathbf{2}Me^{2+}$ have been synthesized according to previously published procedures.[26] Commercially available compounds were reagent grade quality and were used without further purification. Solvents for spectroscopic measurements were of spectroscopic grade (Merck-Uvasol); spectroelectochemical measurements were carried out in argon-purged acetonitrile (Romil Hi-DryTM) solutions at room temperature.

Photophysical measurements: UV-vis absorption spectra were recorded with a Perkin Elmer Lambda 45 spectrophotometer using quartz cells with pathlengths of 1.0 cm. The precision on the wavelength values was ± 2 nm. Molar absorption coefficient values were determined using the Lambert-Beer law; the experimental error, mostly due to weighting error, can be estimated to be around 5%. Luminescence spectra were performed with a Perkin Elmer LS-55; the precision on the wavelength values was ± 2 nm. Luminescence quantum yields have been determined on solution samples at room temperature referring to the relative method optimized by Demas and Crosby.[27] Quinine sulphate in 0.5 M H_2SO_4 ($\phi = 0.55$) aqueous solution was used as standard. Excited-state lifetimes were measured with an Edinburgh FLS920 spectrofluorimeter equipped with a TCC900 card for data acquisition in time-correlated single

photon counting mode (0.5 ns time resolution) and with a PicoQuant pulsed diode laser 340 ± 20 nm as an excitation source. The experimental error on lifetime measurements is ± 10 %. Pump-probe transient absorption measurements were performed with an Ultrafast Systems HELIOS (HE-VIS-NIR) femtosecond transient absorption spectrometer by using, as excitation source, a Newport Spectra Physics Solstice-F-1 K-230 V laser system, combined with a TOPAS Prime (TPR-TOPAS–F) optical parametric amplifier (pulse width: 100 fs, 1 kHz repetition rate) tuned at 300 nm. A CaF_2 crystal for continuum generation in the UV-vis range (330-800 nm) has been employed. The overall time resolution of the system is 300 fs. Air-equilibrated solutions in 0.2 cm optical path cells were analyzed under continuous stirring. The pump energy on the sample was 2 μJ/pulse. Surface Xplorer V4 software from Ultrafast Systems was used for data elaboration using single wavelength and single decay analysis on the different sections of the maps. Lifetimes were taken as average of values derived from the fitting of several decays at different wavelengths. Errors on lifetimes were estimated as average of the errors reported by the fitting software for each lifetime. The 3D data surfaces were corrected for the chirp of the probe pulse prior to analysis. Global analysis has been also performed with the same software on the data surfaces, by fixing principal components via single value decomposition and by deriving the spectral distributions of the pre-exponential coefficients of the calculated lifetimes. This analysis did not provide additional information on the spectral assignments of the species involved in excited state deactivation of the studied systems.

Spectroelectrochemical measurements: Experiments were performed in a custom built optically transparent thin-layer electrochemical (OTTLE) cell, having Pt minigrids (ca. 0.3 cm^2) as the working and counter electrodes, and an Ag wire as a pseudo-reference electrode, all melt-sealed into a polyethylene spacer. The thickness of the layer, determined by spectrophotometry, was ca. 180 μm. The electrolysis was controlled by Autolab 30 multipurpose instrument interfaced to a PC, and the absorption spectra were recorded with an Agilent Technologies 8543 diode array spectrophotometer. The electrolysis times were determined on the basis of the spectral changes observed: when no further spectral variations occurred, the electrolysis was stopped.

Computational studies: The calculations were performed with DFT and its time dependent extension TD-DFT[28] with implicit acetonitrile (PCM)[29] as implemented in Gaussian 16.[30] The density functional utilized for the optimization of the conformers in the ground state and in the first excited states and absorption and emission spectra was CAM-B3LYP at the Def2TZVPP basis set level for $\mathbf{2}^{+}$ and $\mathbf{2Me}^{2+}$, and Def2SVPP for the tetramers. For optimization and single points calculations of the S_1 and S_2 excited states, the twelve energetically lowest excited singlet states were used. For the absorption spectroscopic profile, the forty energetically lowest excited states were used. The stationary points in the ground and excited state were characterized by frequency calculations. For SOC (spin orbital coupling) and STEOM-DLPNO-CCSD calculations ORCA 5.0 software package was used.[31]

Supporting Information Summary

The Supporting Information include UV-VIS acid titrations, details on computational studies and spectroelectrochemical traces.

Acknowledgements

Financial support from the University of Bologna and CNR (project Fotochimica) are gratefully acknowledged. P.C. and M. M. acknowledge the University of Bologna for financial support.

Conflict of Interests

The authors declare no conflict of interest.

Data Availability Statement

The data that support the findings of this study are available from the corresponding author upon reasonable request.

Keywords: bipyridinium · pyridyl pyridinium · tetramer · theoretical study · transient absorption

[1] a) W. Zhang, J. S. Moore, *Angew. Chem. Int. Ed.* **2006**, *45*, 4416–4439; *Angew. Chem.* **2006**, *118*, 4524–4548.
[2] J. S. Moore, *Acc. Chem. Res.* **1997**, *30*, 402–413.
[3] G. D. Scholes, K. P. Ghiggino, *J. Photochem. Photobiol A: Chem.* **1994**, *80*, 355–362.
[4] M. Villa, P. Ceroni, A. Fermi, *ChemPlusChem.* **2022**, *87*, e2021005.
[5] A. Amati, P. Cavigli, A. Kahnt, M. T. Indelli, E. Iengo, *J. Phys. Chem. A* **2017**, *121*, 4242–4252.
[6] H. He, S. Lee, N. Liu, X. Zhang, Y. Wang, V. M. Lynch, D. Kim, J. L. Sessler, X.-S. Ke, *J. Am. Chem. Soc.* **2023**, *145(5)*, 3047–3054.
[7] S. Ansteatt, B. Uthe, Mandal, R. S. Gelfand, B. D. Dunietz, M. Pelton, M. Ptaszek *Phys. Chem. Chem. Phys.* **2023**, *25*, 8013–8027.
[8] M. Marchini, M. Baroncini, G. Bergamini, P. Ceroni, M. D'Angelantonio, P. Franchi, M. Lucarini, F. Negri, T. Szreder, M. Venturi, *Chem. Eur. J.* **2017**, *23*, 6380–6390.
[9] Y. Alesanco, J. Palenzuela, R. Tena-Zaera, G. Cabañero, H. Grande, B. Herbig, A. Schmitt, M. Schott, U. Posset, A. Guerfi, M. Dontigny, K. Zaghib, A. Viñuales, *Sol. Energy Mater. Sol. Cells* **2018**, *157*, 624–635.
[10] R. J. Mortimer, T. S. Varley, *Chem. Mater.* **2011**, *23*, 4077–4082.
[11] S. Sen, J. Saraidaridis, S. Y. Kim, G. T. R. Palmore, *ACS Appl. Mater. Interfaces* **2013**, *5*, 7825–7830.
[12] a) J. Li, S. Pudar, H. Yu, S. Li, J. S. Moore, J. Rodríguez-López, N. E. Jackson, C. M. Schroeder, *J. Phys. Chem. C* **2021**, *125*, 21862–21872; b) X. Li, X. Yuan, P. Deng, L. Chen, Y. Ren, C. Wang, L. Wu, W. Feng, B. Gongc, L. Yuan, *Chem. Sci.* **2017**, *8*, 2091–2100.
[13] M. Marchini, A. Luisa, G. Bergamini, N. Armaroli, B. Ventura, M. Baroncini, N. Demitri, E. Iengo, P. Ceroni, *Chem. Eur. J.* **2021**, *27*, 16250–16259.
[14] Q. Zhang, Y. Jin, L. Ma, Y. Zhang, C. Meng, C. Duan, *Angew. Chem.* **2022**, *61*, e202204918.
[15] a) F. Puntoriero, A. Arrigo, A. Santoro, G. La Ganga, F. Tuyeras, S. Campagna, G. Dupeyre, P. P. Laine, *Inorg. Chem.* **2019**, *58*, 5807–5817; b) J. Fortage, C. Peltier, F. Nastasi, F. Puntoriero, F. Tuyèras, S. Griveau, F. Bedioui, C- Adamo, I. Ciofini, S. Campagna, P. P. Lainé, *J. Am. Chem. Soc.* **2010**, *132*, 16700–16713.
[16] G. Bergamini, A. Fermi, M. Marchini, M. Locritani, A. Credi, M. Venturi, F. Negri, P. Ceroni, M. Baroncini, *Chem. Eur. J.* **2014**, *20*, 7054–7060.
[17] In our previous work (see Ref. [8]) the quantum yield of $\mathbf{1}^{4+}$ was reported to be 40 %, the value was estimated in water solution; however, in acetonitrile solution the quantum yield of $\mathbf{1}^{4+}$ is 15 %.
[18] A. Banyasz, L. Martinez-Fernandez, T.-M- Ketola, A. Muñoz-Losa, L. Esposito, D. Markovitsi, R. Improta, *J. Phys. Chem. Lett.* **2016**, *7(11)*, 2020–2023.
[19] In our previous work (ref. [13]), a time constant of 34 ps was measured for the same process. The discrepancy can be given by a more accurate analysis, performed in the present work, that considered a larger probe spectral area.
[20] J. Peon, X. Tan, J. D. Hoerner, C. Xia, Y. Fei Luk, B. Kohler, *J. Phys. Chem. A* **2001**, *105(24)*, 5768–5777.

[21] J. A. Farrington, M. Ebert, E. J. Land, *J. Chem. Soc. Faraday Trans. 1* **1978**, *74*, 665–675.
[22] M. Villa, P. Ceroni, A. Fermi, *ChemPlusChem* **2022**, *87*, e20210055.
[23] M.-C. Yoon, S. Lee, S. Tokuji, H. Yorimitsu, A. Osuka, D. Kim *Chem. Sci.* **2013**, *4*, 1756–1764.
[24] S. Sengupta, S. K. Sadhukhan, *Indian J. Chem. Sect. B* **2003**, *42*, 858–862.
[25] S. Sengupta, S. K. Sadhukhan, S. Muhuri, *Tetrahedron Lett.* **2002**, *43*, 3521–3524.
[26] a) M. Marchini, M. Baroncini, G. Bergamini, P. Ceroni, M. D'Angelantonio, P. Franchi, M. Lucarini, F. Negri, T. Szreder, M. Venturi, *Chem. Eur. J.* **2017**, *23*, 6380–6390; b) G. Bergamini, A. Fermi, M. Marchini, M. Locritani, A. Credi, M. Venturi, F. Negri, P. Ceroni, M. Baroncini, *Chem. Eur. J.* **2014**, *20*, 7054–7060.
[27] G. A. Crosby, J. N. Demas, *Rev. J. Phys. Chem.* **1971**, *75*, 991–1024.
[28] M. Caricato, B. Mennucci, J. Tomasi, F. Ingrosso, R. Cammi, S. Corni, G. Scalmani, *J. Chem. Phys.* **2006**, *124*, 124520.
[29] J. Tomasi, B. Mennucci, R. Cammi, *Chem. Rev.* **2005**, *105*, 2999–3094.
[30] M. J. Frisch, G. W. Trucks, H. B. Schlegel, G. E. Scuseria, M. a. Robb, J. R. Cheeseman, G. Scalmani, V. Barone, G. a. Petersson, H. Nakatsuji, X. Li, M. Caricato, V. Marenich, J. Bloino, B. G. Janesko, R. Gomperts, B. Mennucci, H. P. Hratchian, J. V. Ortiz, a. F. Izmaylov, J. L. Sonnenberg, Williams, F. Ding, F. Lipparini, F. Egidi, J. Goings, B. Peng, A. Petrone, T. Henderson, D. Ranasinghe, V. G. Zakrzewski, J. Gao, N. Rega, G. Zheng, W. Liang, M. Hada, M. Ehara, K. Toyota, R. Fukuda, J. Hasegawa, M. Ishida, T. Nakajima, Y. Honda, O. Kitao, H. Nakai, T. Vreven, K. Throssell, J. a. Montgomery Jr., J. E. Peralta, F. Ogliaro, M. J. Bearpark, J. J. Heyd, E. N. Brothers, K. N. Kudin, V. N. Staroverov, T. a. Keith, R. Kobayashi, J. Normand, K. Raghavachari, a. P. Rendell, J. C. Burant, S. S. Iyengar, J. Tomasi, M. Cossi, J. M. Millam, M. Klene, C. Adamo, R. Cammi, J. W. Ochterski, R. L. Martin, K. Morokuma, O. Farkas, J. B. Foresman, D. J. Fox, *Gaussian, Inc., Wallin*, **2016**.
[31] a) F. Neese, "The ORCA program system" *Wiley Interdisciplinary Reviews: Computational Molecular Science*, **2012**, Vol. 2, Issue 1, 73–78; b) F. Neese, "Software update: the ORCA program system, version 4.0" *Wiley Interdisciplinary Reviews: Computational Molecular Science*, **2017**, Vol. 8, Issue 1, e1327.

Manuscript received: June 9, 2023
Accepted manuscript online: August 10, 2023
Version of record online: September 28, 2023